THE JOURNAL OF PHYSICAL CHEMISTRY C

Article

pubs.acs.org/JPCC

# Preparation, Characterization, and Electronic Structure of Asymmetric Isonaphthalimide: Mechanism of Dual Fluorescence in Solid State

Eduard V. Ganin,[†] Artëm E. Masunov,*[,‡] Anatolii V. Siminel,[§] and Marina S. Fonari*[,§]

[†]Odessa State Environmental University, Lvovskaya str. 15, 65016 Odessa, Ukraine

[‡]NanoScience Technology Center, Department of Chemistry, Department of Physics, and Florida Solar Energy Center, University of Central Florida, Orlando, Florida 32826, United States

[§]Institute of Applied Physics ASM, Academy str. 5, MD2028 Chisinau, Moldova

Supporting Information

**ABSTRACT:** The asymmetric isonaphthalene imide, 3-[(4-nitrophenyl)imino]-1*H*,3*H*-benzo[*de*]isochromen-1-one was obtained by condensation of 1,8-naphthoylchloride with *p*-nitroaniline in the presence of pyridine. The crystal structure and vibrational and electronic absorption spectra are reported. The emission spectrum of the crystalline phase demonstrates dual luminescence, with short and long wavelength components, while only the short wavelength component is present in chloroform solution. The geometrical and electronic structures of the ground and excited states of the molecule are investigated using density functional theory methods. Dual fluorescence is explained in terms of the excited states of different nature. The spectroscopic properties of newly synthesized compounds for possible biosensor applications are discussed.

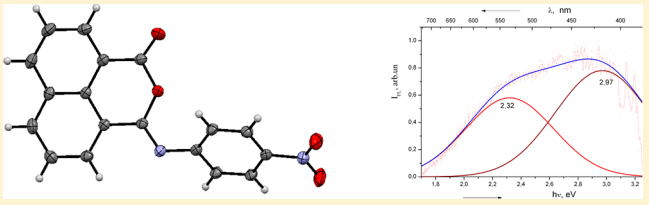


## INTRODUCTION

Core-substituted naphthaldiimides and their derivatives with an extended $\pi$-conjugated system represent a rapidly emerging area due to their applications in functional nanomaterials and implications in biological and supramolecular arrays.[1,2] On the other hand, acylation of amines by derivatives of carboxylic acids results in *O*-acylimidates, including isoimides that represent the labile intermediates and act as precursors in the synthesis of thermodynamically more stable *N*-acylimidates, i.e., imides.[3,4] According to the previously reported data,[5,6] interaction of 1,8-naphthaloylchloride with anilines resulted in yellow symmetric chromophores, *N*-phenylnaphthalimides **Ia,b.** However, taking into account the reported records about condensation products between phthaloylchloride and amines,[7−9] those findings look ambiguous, as far as the isomeric asymmetric *N*-phenylisonaphthalimides **IIa,b** might also been expected (Scheme 1).

**Scheme 1. Structural Formulas for Symmetric *N*-Phenylnaphthalimides Ia,b and Asymmetric *N*-Phenylisonaphthalimides IIa,b**

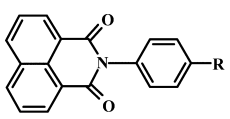

**Ia,b**

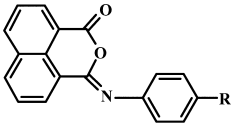

**IIa,b,** where R = H, $NO_2$

Since in recent years naphthalimide derivatives are increasingly used as fluorescent dyes,[1,10−16] isonaphthalimides that possess possible higher reactivity due to their asymmetric structure in comparison with the symmetric naphthalimides are of keen interest as precursors in the synthesis of such materials. With the aim to disclose the actual structure of the interaction product of 1,8-naphthaloylchloride with anilines, we reproduced the reported earlier experimental conditions[4] using *p*-nitroaniline as a starting agent (Scheme 2). This contribution

**Scheme 2. Synthesis of IIb**

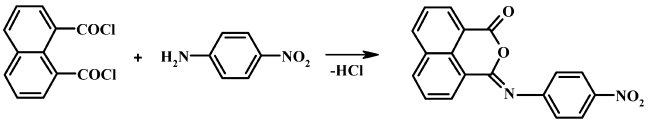

**IIb**

summarizes the synthesis and X-ray structural evidence for the asymmetric isonapthalimide, 3-[(4-nitrophenyl)imino]-1*H*,3*H*-benzo[*de*]isochromen-1-one **IIb**, and provides an overview based on DFT computations of the experimentally detected dual luminescence of the crystalline phase on the studied compound that has never before been observed. The reported claims can lead to the development of better fluorescent dyes

**Received:** February 26, 2013
**Revised:** July 3, 2013
**Published:** August 6, 2013






dx.doi.org/10.1021/jp402016j | *J. Phys. Chem. C* 2013, 117, 18154−18162

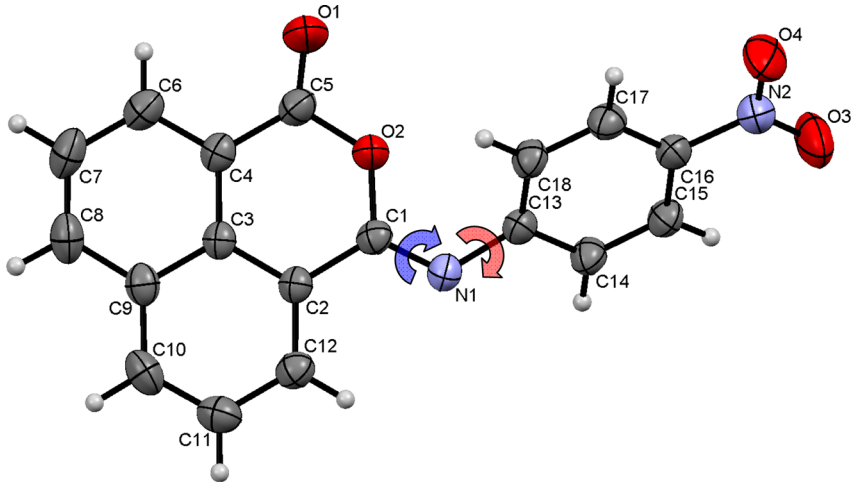


**Figure 1.** ORTEP representation of **IIb** with numbering scheme. Thermal ellipsoids are drawn at 50% probability level. Selected bond lengths (Å): O(1)−C(5) 1.194(2); O(2)−C(1) 1.375(2); O(2)−C(5) 1.379(2); N(1)−C(1) 1.263(2); N(1)−C(13) 1.407(2); O(3)−N(2) 1.222(2); O(4)−N(2) 1.216(2); N(2)−C(16) 1.455(3) Å. The pink and blue arrows indicate two dihedral angles that determine the molecular conformation: C(18)−C(13)−N(1)−C(1) and C(13)−N(1)−C(1)−O(2), respectively (experimental values are 51.9(3)° and 6.4(3)°).

while contributing to the theoretical understanding of this group of compounds.

## EXPERIMENTAL SECTION

**1. General Considerations.** Reaction monitoring was carried out by TLC on the Silufol UV-254 plates, eluting in the acetone hexane = 1:10 with developing by ninhydrin. Spots were detected under ultraviolet light. The IR spectrum was obtained on the instrument Perkin-Elmer 580B in a tablet with KBr. The mass spectrum was obtained on the MAT 112 instrument at 70 eV ionizing voltage with a direct input into the source of the sample, sample evaporation temperature 20−70 °C, and temperature of the ionization chamber 220−230 °C.

**2. Synthesis.** *N*-(4-Nitrophenyl)isonaphthalimide **IIb** was obtained according to the published procedure[4] by interaction of 1,8-naphthoylchloride with 4-nitroaniline in boiling benzene (yield 50%) and by modified technique given herein. 1,8-Naphthoylchloride (0.01 mol) dissolved in 100 mL of benzene, with stirring, was poured in 100 mL of benzene solution of 4-nitroaniline (0.015 mol) and pyridine (0.03 mol). The reaction mixture was kept for 20 min and washed with 200 mL of 3% hydrochloric acid, 3 × 200 mL of water, and the benzene was then distilled off, and isonaphthalene imide **IIb** was isolated by crystallization. The yield of yellow crystalline solid is 95%. Final product is insoluble in water, methanol, ethanol, hexane, and ethylacetate and soluble in chloroform upon heating. Mp 262−263 °C (from acetone). Anal. Calcd for $C_{18}H_{10}N_2O_4$: C(67.92%), H(3.17%), N(8.80%). Found: C(67.87%), H(3.10%) N(8.85%). IR ($\nu$, $cm^{-1}$): 3395, 3111, 2922, 2871, 1754 (C═O), 1653 (C═N), 1582($\nu^{as}NO_2$), 1501, 1488, 1335($\nu^{s}NO_2$), 1314, 1296, 1216, 1108, 1037 (C−O−C), 877, 839, 770, 753, 700, 680. Molecular ion: ($M^+$): 318 a.e.M.

**3. X-ray Crystallography.** A yellow crystal of compound **IIb** was mounted on a Xcalibur Oxford Diffraction CCD diffractometer equipped with a graphite monochromator. Data collection was performed at ambient conditions using MoK$\alpha$ radiation. The structure was solved by direct methods using the program SHELXS-97 and refined by full matrix least-squares on $F^2$ with SHELXL-97.[17] All nonhydrogen atoms were refined anisotropically. All hydrogen atoms were included in calculated positions and treated as riding atoms using SHELXL-97 default parameters. An empirical absorption correction using spherical harmonics implemented in SCALE3 ABSPACK scaling algorithm was applied. Crystallographic data for **IIb**: $C_{18}H_{10}N_2O_4$, monoclinic, space group $C2/c$, $a$ = 29.360(3), $b$ = 3.8228(3), $c$ = 24.968(2) Å, $\beta$ = 93.109(10)°, $V$ = 2798.2(4) Å$^3$, $Z$ = 8, $M$ = 318.28, $D$calc = 1.511 g cm$^{-3}$, GOF = 1.011, $R_1$ = 0.0486, $wR_2$ = 0.1071, for 1886 reflections with $I > 2\sigma(I)$; $R_1$ = 0.0778, $wR_2$ = 0.1266, for all 2744 independent reflections. Crystallographic data (excluding structure factors) for the structure have been deposited at the Cambridge Crystallographic Data Centre (CCDC) as supplementary publication No. CCDC 916517.

**4. Electronic Spectroscopy.** UV−vis absorption spectrum was recorded on Perkin-Elmer UV−vis Lambda-25 spectrometer at room temperature. Emission spectrum was measured for monocrystals at room temperature on an Excitation YAG:$Nd^{3+}$ laser, third harmonic generation, $\lambda$ = 355 nm, duration = 10 ns, time repetition 15 Hz, impulse energy 0.3 kJ. The emission was registered by a FEU-79 output amplifier; the proper time of the recording system is 10 ns. Fluorescence decay curves were measured in the solid form and in chloroform solution. Experimental lifetimes, obtained from the fitting of the fluorescence decay curves, were found to be 20 ± 0.3 and 25 ± 0.3 ns for the solid and solution forms respectively. Fluorescence quantum yields, Φ, were measured using the standard method of comparison with a known "red" standard dye, Cresyl Violet perchlorate (Sigma Aldrich) in methanol, which has an absorption peak at 594 nm, fluorescence peak at 620 nm, and a quantum yield of 0.54. For both solid and solution forms, the Φ were found to be low on the order of 0.01.

## RESULTS AND DISCUSSION

Two absorption bands at 1754 and 1653 $cm^{-1}$ in the IR spectrum of the resulting yellow compound, being similar to those found for the five-membered isophthalimides,[4,7] indicate in favor of the isonaphthalimide structure **IIb**. As far as the retrieval of CSD (version 5.34 November 2012, one update)[18] revealed no examples of six-membered isoimides, the single crystal X-ray diffraction study has been undertaken, and the


dx.doi.org/10.1021/jp402016j | J. Phys. Chem. C 2013, 117, 18154−18162

final product has been identified as the asymmetric *n*-(4-nitrophenyl)isonaphthalene imide **IIb**.

**1. Crystal Structure.** Compound **IIb** crystallizes in the monoclinic space group *C*2/*c* with one molecule per asymmetric unit. The molecular structure with selected bond distances is shown in Figure 1. The structural parameters of planar tricylic core for **IIb** are comparable with those found for 1,8-naphthalic anhydride and 3-(4,5-ethylenedithio-1,3-dithiol-2-ylidene)naphthopyranone.[19] The *N*-attached *p*-nitrophenyl moiety exhibits a nearly planar geometry with the dihedral angle between the aromatic ring and nitro group of 4.0(2)°. The whole molecule adopts an angular shape with the dihedral angle C(18)−C(13)−N(1)−C(1) of 51.9(3)° that minimizes the steric hindrance as the H(C18)...O(2) separation of 2.62 Å indicates.

In the crystal, the molecules stack along the *b*-axis in a herringbone type arrangement (Figure 2). The interplanar separations between the aromatic moieties in stacks are equal to 3.407 Å between tricyclic cores and 3.511 Å between the phenyl rings of 4-nitrophenyl substituents.

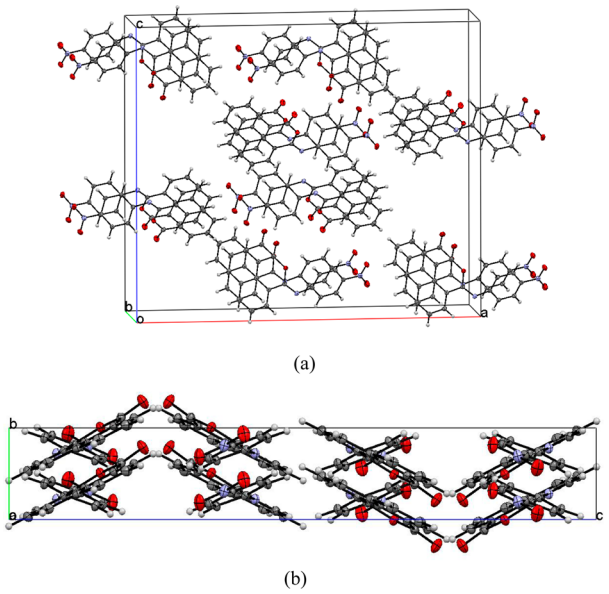


**Figure 2.** Packing of **IIb** molecules. Views along *b*- (a) and *a*-axes (b).

**2. Emission Spectra.** The most intriguing optical property of **IIb** found in the present study is dual fluorescence in the solid state (Figure 3). The shape of the emission curve indicates a superposition of at least two bands with peaks at 2.99 eV (420 nm) and 2.39 eV (525 nm). Of the most commonly used Alentsev−Fock and Gaussian methods the latter was employed for spectrum resolution herein.[20] To our knowledge, such phenomenon was not previously reported, although dual fluorescence in solution of other naphthaleneimides is well documented.[21,22]

As many as 11 different mechanisms of dual fluorescence were identified in the literature.[23] All these mechanisms can be classified into three groups: tautomerism, conformational change, and excimer/exciplex formation. The dual fluorescence with the low quantum yield is typical for polar solutions of naphthalimides.[21] Previously published studies of dual fluorescence from naphthalimides under pressure reported an increase in quantum yield in the solvents with increased viscosity and were interpreted as emission from planar and twisted intramolecular charge transfer (TICT) states.[22] Hindering the twisting motion upon geometrical relaxation of TICT state decreases intersystem crossing rates into the triplet state and improves fluorescence quantum yield. Similar effects were reported for related chromophores upon hydrogen bond formation[24] and DNA intercalation.[25,26] Potential sensitivity to the molecular environment makes the new class of compounds prime candidates for future biosensor and anticancer[28] activity studies.

**3. Computational Studies of Optical Properties and Potential Energy Surfaces.** In order to obtain deeper understanding of the electronic structure, optical, and conformational properties of **IIb**, we performed a series of quantum chemical calculations using DFT and TD-DFT methods. All calculations employed the Gaussian 2009 suite of programs.[29] We elected to use range-separated hybrid exchange correlation functional CAM-B3LYP,[30] which was designed to improve the description of the states with

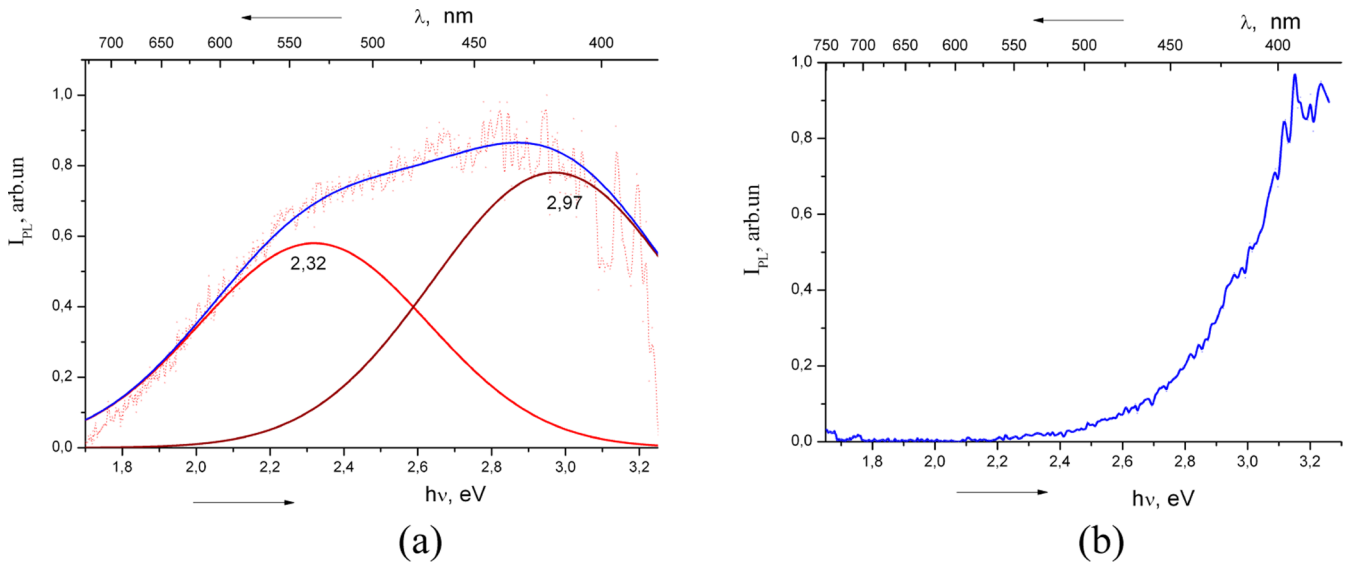


**Figure 3.** Solid-state (a) and solution (b) emission spectrum for **IIb** at room temperature. Red and brown lines, elementary bands.


dx.doi.org/10.1021/jp402016j | *J. Phys. Chem. C* 2013, 117, 18154−18162

**Table 1. Properties of the Seven Lowest States in IIb Monomers, Dimers, and Trimers: Vertical Absorption Energy ($E$, eV), Absorption Wavelengths ($\lambda$, nm), and Oscillator Strengths ($f$)**

| | experiment | monomer | | | dimer | | | trimer | | |
|---|---|---|---|---|---|---|---|---|---|---|
| | $\lambda$ | $E$ | $\lambda$ | $f$ | $E$ | $\lambda$ | $f$ | $E$ | $\lambda$ | $f$ |
| $S_1$ | 361 | 3.73 | 332 | 0.975 | 3.67 | 337 | 0.023 | 3.59 | 344 | 0.089 |
| $S_2$ | | 4.06 | 304 | 0.000 | 3.69 | 335 | 1.456 | 3.68 | 336 | 0.014 |
| $S_3$ | | 4.31 | 287 | 0.066 | 4.05 | 305 | 0.000 | 3.71 | 333 | 0.581 |
| $S_4$ | | 4.37 | 283 | 0.120 | 4.05 | 305 | 0.001 | 3.91 | 316 | 0.000 |
| $S_5$ | | 4.67 | 265 | 0.000 | 4.13 | 299 | 0.074 | 3.92 | 315 | 0.000 |
| $S_6$ | 268 | 4.70 | 263 | 0.169 | 4.25 | 291 | 0.332 | 3.94 | 314 | 0.000 |
| $S_7$ | | 4.84 | 255 | 0.017 | 4.30 | 288 | 0.009 | 4.02 | 308 | 0.047 |

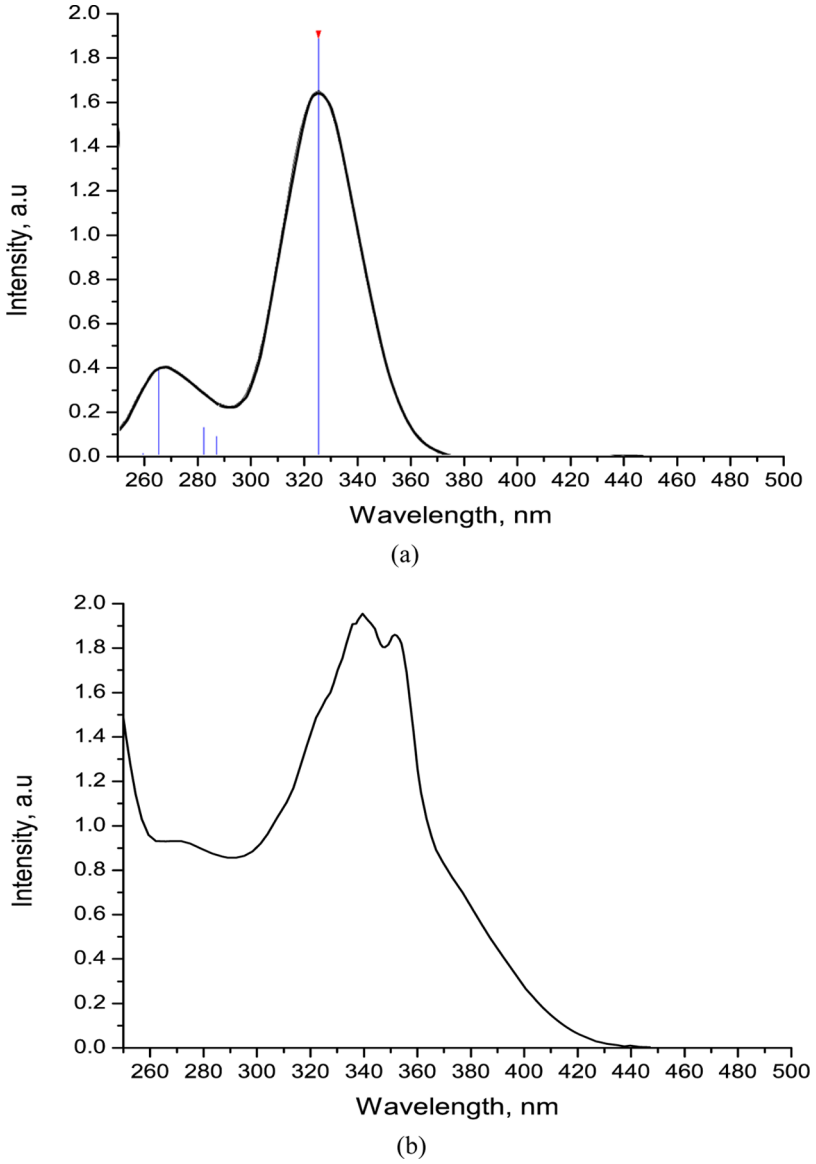


**Figure 4.** Theoretical (a) and experimental (b) absorption spectra of **IIb** in chloroform.

substantial charge transfer character. It is worth noting that the more popular functionals with low Hartree−Fock exchange, such as B3LYP or PBE0, overestimate the emission wavelengths more than twice in some cases with strong charge transfer (such as nitro and amino substitutes dyes) and require empirical linear regression correction in order to produce results comparable with experimental emission wavelength in naphthalimide derivatives.[31] The solvent effect of the chloroform was taken into account using polarizable continuum model (PCM) in recent solvent model density (SMD) parametrization.[32] The ground state geometry of **IIb** was optimized at the CAM-B3LYP/6-31G*/PCM theory level, and the vertical electronic transitions were predicted in this geometry at TD-CAM-B3LYP/6-31G*/PCM theory level. The energies, corresponding wavelengths, and oscillator strengths (proportional to the absorption intensities and


dx.doi.org/10.1021/jp402016j | J. Phys. Chem. C 2013, 117, 18154−18162

inversely proportional to the radiative lifetimes) of the seven lowest singlet excited states are presented in Table 1, while spectra broadened with empirical 0.33 eV line widths are shown in Figure 4a. One can see that the multiple maximum observed at 340−350 nm corresponds to absorption into $S_1$ state, which has the largest oscillator strength and will be called "bright state" $S_b$ in the following. The vibronic structure of the absorption band, partially resolved in experiment, was not taken into account in DFT simulations. The shoulder at 330 nm corresponds to absorption into $S_3$ and $S_4$ states, which are too close to be separated, while $S_6$ state with the second largest oscillator strength corresponds to the short wavelength peak observed at 268 nm. The second excited singlet $S_2$ has low oscillator strength (which will be called "dark state", $S_d$) and is nearly degenerate with $S_b$. Therefore, these two states may result in dual fluorescence and will be analyzed in detail below.

The bright state $S_b$ presents essentially HOMO to LUMO transition of $\pi\pi^*$ nature. Examination of the Kohn−Sham orbitals, involved in this transition (Figure 5b,c) allows one to conclude that both HOMO and LUMO are delocalized over the whole molecule (except for the $NO_2$ group in the case of HOMO). Therefore, the excitation into state $S_b$ is accompanied by a weak charge transfer onto the nitro group. This conclusion is supported by the value of the permanent dipole moment for this state (15.3 D), which is slightly higher than the ground state dipole moment of 14.4 D. The dark state $S_d$ presents predominantly HOMO−1 to LUMO transition of $n\pi^*$ nature (see Figure 5a,c). Upon excitation into $S_d$ the electron density is transferred from the oxygen lone pairs localized on the nitro group into LUMO, delocalized over the whole molecule. As a result of the charge transfer from the nitro group to the rest of the molecule, the permanent dipole moment for this state (11.5 D) is reduced in comparison to the ground state moment.

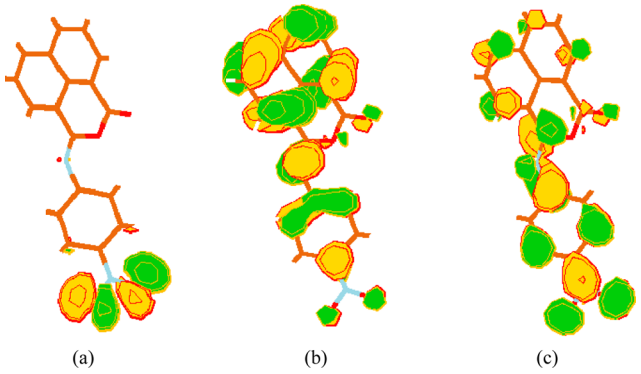


**Figure 5.** Essential Kohn−Sham orbitals of the **IIb** in the dark excited state optimized geometry: (a) HOMO−1; (b) HOMO; (c) LUMO.

Prediction of the emission spectra requires the geometry optimization of the excited states. If the states $S_b$ and $S_d$ had distinctly different geometries, with the dark $S_d$ corresponding to a deeper energy minimum, this could explain the emission at two distinct wavelengths, similar to the one observed in polar solutions of *N*-phenylnaphthalimides.[22] In those systems, the origin of dual fluorescence was explained by the quick conversion of the strongly emitting planar bright state into twisted charge transfer state, which is more stable but emits weakly. One could expect similar nature of dual fluorescence in the case of **IIb**. In order to test this hypothesis, we performed the relaxed scan and plotted the potential energy curve (also known as minimum energy profile, MEP) in Figure 6a. All internal coordinates were optimized during this scan, except for two dihedral angles marked with the curved arrows in Figure 1: CCNC (twisting of the nitrophenyl ring) and CNCO (twisting of the fused naphthalene ring). The {CCNC_CNCO} notation will be used in the following discussion to identify the conformation. As one can see from Figure 6a, the $S_0$ ground state energy is relatively insensitive to the twisting of the CCNC dihedral (rotation about single N−C bond, scan points 1−10 in Figure 6a) with the shallow minimum corresponding to {50_04}, fairly close to experimental values {52_06}. Twisting of the CNCO dihedral angle (rotation about double N═C bond, scan points 11−21 in Figure 6a) is associated with substantial energy barrier (about 25 kcal/mol). The top of the barrier appears to be flat, as the CNC angle approaches 180°, and potential energy becomes insensitive to the changes in the dihedrals. Increase of the CNCO dihedral angle beyond 90° (scan points 11−21 in Figure 6a) is leading to another energy minimum that corresponds to the *cis*-conformation of **IIb**. Optimization of the CCNC dihedral on this interval was necessary to minimize the steric repulsion. The *cis*-conformation is separated from the *trans*-conformation with ground state energy barrier of nearly 11 kcal/mol. The profile of the dark state $S_d$ is very similar. The global minimum corresponds to {54.7_3.5} for the ground and {38_2.7} for the dark excited state, fairly close to the crystallographic conformation {52_6.4}. The metastable *cis*-conformation corresponds to the local minimum at {83_180} for the ground and {42.6_180} for the dark singlet states. The bright excited state $S_b$, on the other hand, has a steep slope from the Franck−Condon geometry toward planarization of CCNC dihedral, and further toward the twist of CNCO dihedral, the only minimum is achieved at the orthogonally twisted conformation {0_90} with the permanent dipole moment of 5.56 D. This indicates much stronger charge transfer into the nitro group than that predicted for this state in the optimized ground state geometry. In addition, the oscillator strength in the optimized geometry of the $S_b$ state is reduced sharply to the value of 0.002 from the value of 1.125 in the ground state optimized geometry. This explains the low emission quantum yield of **IIb**.

These changes in the oscillator strengths can be explained with the help of the natural orbitals of the excited states (Figure 7). While the absorbing state ($S_b$ at $S_0$ geometry) presents transition between two delocalized $\pi$-orbitals, its relaxation results in localization of the transition on the imido bridge. Hence, the nature of this state changes into $n$(N)−$\pi^*$(C═N) with a large twist along C═N bond and low oscillator strength. The $S_d$ state, on the other hand, retains $n(NO_2)-\pi^*$ nature and the low oscillator strength upon its relaxation (which consists of planarization in this case).

The predicted emission wavelength in the optimized geometry of the bright state is 813 nm, far from the weak emission at 390 nm observed in chloroform solution. One can speculate that the major channel of the bright state decay is radiationless. This is supported by the MEP of the triplet state, obtained at U-CAM-B3LYP/6-31G* theory level and presented by the black circles in Figure 6. The singly occupied orbitals in this state (not shown) are similar to the essential orbitals of the dark state (Figure 5b,c). As one can see, at the twisted conformation {0_90} (point 20 on Figure 6a) the energies of $S_b$ and $T_1$ states approach each other closely, drastically increasing the probability of intersystem crossing. Although we did not attempt to estimate spin−orbit coupling matrix elements in this study, the sizable value of this matrix element


dx.doi.org/10.1021/jp402016j | J. Phys. Chem. C 2013, 117, 18154−18162

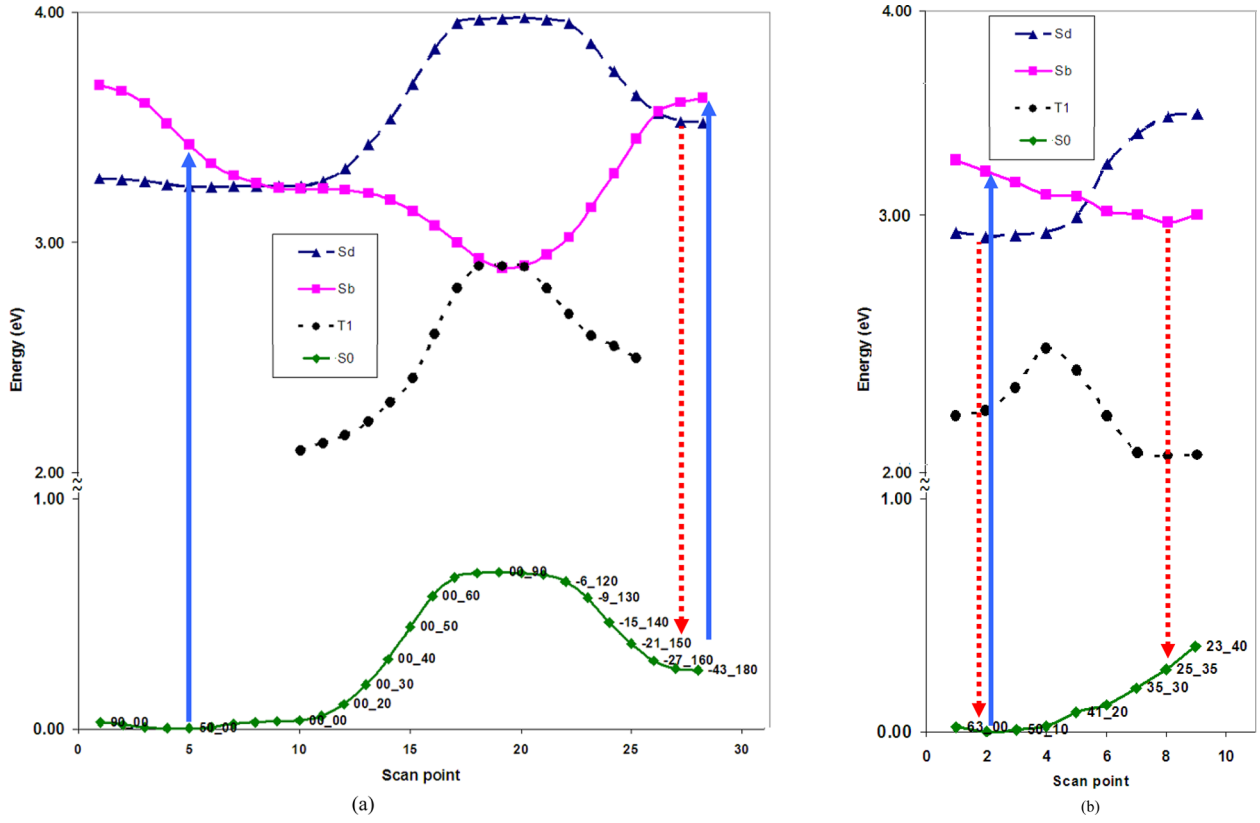


**Figure 6.** Minimum energy profiles (in eV) for the molecule (a) and stacking trimer (b) of **IIb**: the ground singlet $S_0$ (solid green line), the lowest triplet $T_1$ (dotted black line), and two singlet excited states: the bright $S_b$ (solid pink line) and the dark $S_d$ (dotted blue line), as a function of dihedral twist (labeled by two angle values at the bottom line). Solid blue lines arrows indicate absorption, dotted red arrow indicates emission.

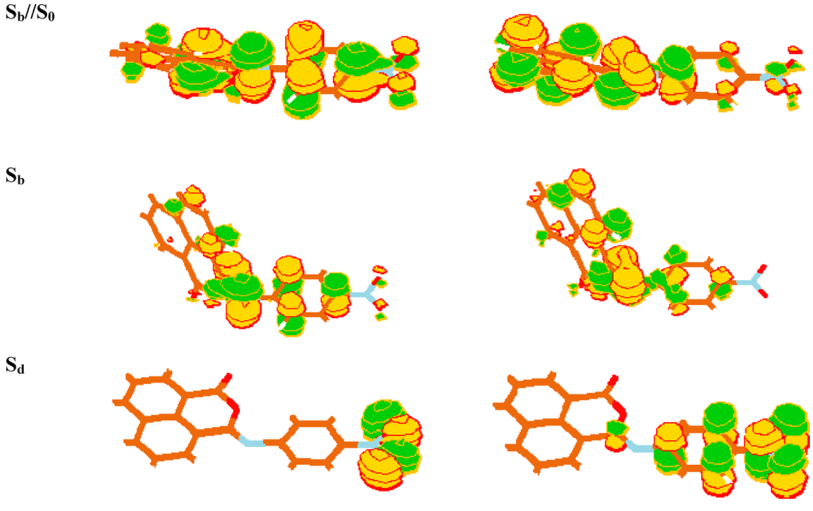


**Figure 7.** Transition natural orbitals for the absorbing state ($S_b$ in $S_0$ geometry, $S_b//S_0$), and relaxed excited states ($S_b$ and $S_d$): the electron transfer occurs from the left (hole) to the right (particle) orbitals.

is expected from $n\pi^*$ and $\pi\pi^*$ nature of the $T_1$ and $S_b$ states and the El Sayed rule.[33] From a close inspection of Figure 6, one can see that the dark state MEP crosses the bright state MEP at two points, close to the *trans*- and *cis*-conformations: {30_0} and {-21_150} (points 9 and 28 in Figure 6a). This indicates the approximate location of the conical intersections, where internal conversion between the singlet states can take place rapidly. However, the dark singlet MEP is flat at the crossing point in the *trans*-conformation. Therefore, *trans*-$S_d$ species do not accumulate long enough to emit light and convert quickly back to the $S_b$ state to continue their geometric relaxation. The radiationless decay from the twist-$S_d$ results in appreciable concentration of the *cis*-conformation of the ground state. The absorption wavelength in this conformation is fairly close to the one of *trans*-conformation, which makes it difficult to verify this prediction experimentally. However, the light absorption by *cis*-$S_0$ leads to excitation into $S_b$ state, close to the vicinity of the $S_b/S_d$ intersection. The *cis*-conformation of $S_d$ is separated from the intersection point by 1 kcal/mol barrier, sufficient to accumulate these species for the picosecond


dx.doi.org/10.1021/jp402016j | J. Phys. Chem. C 2013, 117, 18154−18162

lifetime necessary for them to emit. We predict the emission of *cis*-$S_d$ to have 370 nm wavelength, close to the experimentally observed 390 nm.

Next we will move to simulate the solid state spectra. In order to investigate the possibility of excimer formation, we performed the computational modeling of the seven lowest excited states of the stacking molecular dimer taken from the crystal structure. The results are presented in Table 1 and Figure 1S. Detailed orbital analysis (Figures 2S and 3S) reveals that the dimer states $S_1$ and $S_2$ originate in splitting of the bright monomer state $S_b$, while the dimer states $S_3$ and $S_4$ result from the splitting of the dark monomer state $S_d$. The oscillator strengths distribution between the $S_1$ and $S_2$ states indicates H-aggregate nature of this stacking dimer, although the energy splitting between these states is very low (2 nm). The splitting typically increases to the detectable values when interacting chromophores have ionic nature.[34] Results of the geometry optimization for each of the excited dimers (not shown) reveal that the excited states can be separated into two groups: the bright states ($S_1$, $S_2$, $S_7$), which emit in short wavelength range (420−460 nm), and the dark states ($S_3$, $S_4$), which are strongly stabilized and emit in long wavelength range (620−660 nm). The reasons why both the bright and the dark states emit light with comparable quantum yield is not clear from the dimer model. However, the orbital analysis (Figures 4S and 5S) demonstrates that electronic excitation in the representative states $S_2$ and $S_3$ is completely localized upon geometric relaxation and their electronic structure is almost identical to the states $S_b$ and $S_d$ of the monomer. The reason for extra stabilization of the dark state is the proximity of the second molecule in the dimer. Specifically, two nitro groups with the large negative charge are positioned at a short distance from each other. This destabilizes the ground and the bright excited state, resulting in relative stabilization of the dark state. The localization of the excitation on one of the two branches of $\pi$-stacking dimer is fairly common.[35] Hence, the formation of excimer in **IIb** crystal where the excitation is localized over two or more molecules is not supported by our simulations.

In order to investigate the detailed mechanism of the molecular packing effects on the excited state processes in the crystal, we used TD-CAM-B3LYP/6-31G* level of theory to predict the minimum energy profiles for the $S_0$, $S_b$, $S_d$, and $T_1$ states in the stacking trimer. The terminal molecules were frozen at their experimental X-ray coordinates, while the central molecule was optimized with CNCO dihedral fixed at nine values between 0° and 40°. Values of the other dihedral CCNC were optimized. They appeared to be largely determined by the steric repulsion between the central and the terminal monomers and were found to be similar in the ground and all the excited states. The values for the ground state are shown as labels next to MEP data points in Figure 6b. The minimum energy profiles display the pattern that is entirely different from the free molecule MEP in Figure 6a. One can see that after the light absorption in the Franck−Condon region {50_04} the trimer can relax along the bright state MEP into a minimum at {25_35}, where it emits a photon. The vertical emission energy was found to be 2.54 eV (488 nm emission wavelength). Alternatively, the system can undergo internal conversion into the dark state at the crossing point close to {41_20}, which is located 0.1 eV (2.7 kcal/mol) above the bright state minimum. After internal conversion, the system can relax into the dark state minimum at {57_05}, which is nearly 5 kcal/mol below the crossing point. This minimum is also well above the triplet surface. These two factors allow for a lifetime of the dark state to be long enough to emit a photon with vertical energy 2.13 eV (corresponding to 582 nm wavelength). Thus, our trimer model of the crystalline material allows us to qualitatively explain its dual fluorescence, while quantitative predictions are both red-shifted by 0.4 eV.

## CONCLUSIONS

In conclusion, the asymmetric isonaphthalene imide 3-[(4-nitrophenyl)imino]-1*H*,3*H*-benzo[*de*]isochromen-1-one obtained as a product of 1,8-naphthoylchloride coupling with *p*-nitroaniline represents the perspective candidate for future studies in biological systems and materials science applications.[27,28,36] The reported data on structure and absorption properties of this compound can be useful also in the synthesis of dyes and luminophores[37] including the modified lariate crown ethers, similar to those for *N*-substituted isophthalimides[38,39] using this luminophore as a side substituent attached to the macrocyclic backbone to provide the spectroscopic response in the complexation reactions.

The new compound was characterized by single crystal X-ray diffraction, FTIR and UV−vis absorption spectroscopy, as well as emission spectroscopy in the solid and chloroform solution. In the crystal, the molecules stack in columns. The interplanar separations between the aromatic moieties in stacks are equal to 3.407 Å between the tricyclic cores and 3.511 Å between the phenyl rings of 4-nitrophenyl substituents. The dual fluorescence with low quantum yield was observed from crystalline material. Quantum chemical simulations using time-dependent density functional theory and CAM-B3LYP functional predict the dark n$\pi$* and the bright $\pi\pi$* excited states with substantial charge transfer character to differ in geometry from each other and from the ground state. Unlike well-studied TICT mechanism in naphthaleneimides, where relaxation of the charge transfer dark state results in intramilecular twist, the isonaphthaleneimide molecule studied here has the bright state that relaxes into geometry with 90° intramolecular twist and the dark state that is essentially planar. Experimental geometry in the solid is intermediate between these conformations. The simulations predict that the geometric constraints by the crystalline environment are responsible for the partial geometric relaxation of these states and appearance of the potential barrier separating them. This barrier explains the dual emission observed from both of these states in experiment. At the same time, in solution complete relaxation of the bright state into twisted conformation is predicted. This twisted conformation undergoes nonradiative deactivation and does not contribute to the emission spectrum. The weak, blue-shifted fluorescence signal detected in chloroform solution can therefore originate from the dark, nearly planar n$\pi$* state, trapped in *cis*-conformation.

## ASSOCIATED CONTENT

### Supporting Information

IR spectrum, crystallographic information (cif file), images for dark and bright optimized states. This material is available free of charge via the Internet at http://pubs.acs.org.

## AUTHOR INFORMATION

### Corresponding Author

*E-mail: amasunov@ucf.edu (A.E.M.); fonari.xray@phys.asm.md (M.S.F.).

### Notes

The authors declare no competing financial interest.

## ■ ACKNOWLEDGMENTS

The authors gratefully acknowledge the advice of anonymous Reviewers and assistance of Dr. hab. Aculina Aricu for spectroscopic support. This work was supported in part by the National Science Foundation (CHE-0832622). Research was performed in part using Stokes HPCC facility at UCF Institute for Simulation and Training (IST) and the National Energy Research Scientific Computing Center (NERSC), a DOE Office of Science user facility at Lawrence Berkeley National Laboratory.

## ■ REFERENCES

(1) Bhosale, S. V.; Bhosale, S. V.; Bhargava, S. K. Recent Progress of Core-Substituted Naphthalenediimides: Highlights from 2010. *Org. Biomol. Chem.* **2012**, *10*, 6455−6468.

(2) (a) Thalacker, C.; Röger, C.; Würthner, F. Synthesis and Optical and Redox Properties of Core-Substituted Naphthalene Diimide Dyes. *J. Org. Chem.* **2006**, *71*, 8098−8105. (b) Röger, C.; Würthner, F. Core-Tetrasubstituted Naphthalene Diimides: Synthesis, Optical Properties, and Redox Characteristics. *J. Org. Chem.* **2007**, *72*, 8070−8075.

(3) *Comprehensive Organic Chemistry. The Synthesis and Reactions of Organic Compounds*; Barton, E., Ollis, D., Eds.; Pergamon Press: Oxford, New York, London, Sydney, Paris, Frankfurt, 1979; Vol. 2.

(4) Hargreaves, M. K.; Pritchard, J. G.; Dave, H. R. Cyclic Carboxylic Monoimides. *Chem. Rev.* **1970**, *70*, 439−469.

(5) Mason, F. Derivatives of 1:8-Naphthalic Acid. Part I. The Preparation and Properties of 1:8-Naphthalyl Chloride. *J. Chem. Soc.* **1924**, *125*, 2116−2119.

(6) Khotinskij, E. S.; Matskevitch, R. M. Synthesis of Amino-phenylimides of Naphthalic Acid. *Trudy nauchn.-issled. In-ta khimii Khar'kov Un-ta* **1951**, *9*, 53−57.

(7) Simonov, Yu. A.; Ganin, E. V.; Zavodnik, V. E.; Makarov, V. F. Diisophthalimidoethane. X-Ray Diffraction Evidence for the Structure of the Product of Acylation of 1,2-Diaminoethane with Phthaloyl Chloride. *Chem. Heterocycl. Compd.* **1987**, *10*, 1056−1059.

(8) Jones, P. J. Crystal Structure of 1,8-Diphthaliso-imidonaph-thalene, $C_{26}H_{14}N_2O_4$. *Z. Kristallogr.* **1993**, *208*, 341−343.

(9) Guirado, A.; Zapata, A.; Arellano, C. R. The Reaction of Phthalidylidene Dichloride with Primary Amines. Synthesis and X-ray Molecular Structure of N-Substituted Phthalisoimides. *Tetrahedron* **1997**, *53*, 5305−5324.

(10) Patrick, L. G. F.; Whiting, A. Synthesis of Some Polymerisable Fluorescent Dyes. *Dyes Pigm.* **2002**, *55*, 123−132.

(11) Gharanjig, K.; Ameri, F.; Dadras, F. S.; Khosravi, A. Novel Naphthalimide Based Azo Disperse Dyes for Dyeing of Polyester Fabrics. *Prog. Color Colorants Coat.* **2011**, *4*, 27−37.

(12) Mokhtari, J.; Nouri, M.; Goudarzi, U. Naphthalimide Based Disperse Dyes for Nylon 6 and Polyester (Pet) Fibers: Synthesis and Evaluation of Technical Properties in the Presence of Urea. *Chin. J. Polym. Sci.* **2011**, *29*, 712−718.

(13) Parvizi, P.; Khosravi, A.; Moradiana, S.; Gharanjig, K. Synthesis and Application of Some Alkali-Clearable Azo Disperse Dyes Based on Naphthalimide Derivatives. *J. Chin. Chem. Soc.* **2009**, *56*, 1035−1042.

(14) Prezhdo, O. V.; Uspenskii, B. V.; Prezhdo, V. V.; Boszczyk, W.; Distanov, V. B. Synthesis and Spectral-Luminescent Characteristics of N-Substituted 1,8-Naphthalimides. *Dyes Pigm.* **2007**, *72*, 42−46.

(15) Gan, J.-A.; Song, Q. L.; Hou, X. Y.; Chen, K.; Tian, H. 1,8-Naphthalimides for Non-Doping OLEDs: The Tunable Emission Color from Blue, Green to Red. *J. Physiol. Pharmacol. Adv.*. **2004**, *162*, 399−406.

(16) Sheldrick, G. M. A Short History of SHELX. *Acta Crystallogr.* **2008**, *A64*, 112−122.

(17) Grabchev, I.; Chovelon, J.-M. Photophysical and Photochemical Properties of Green Fluorescent Liquid Crystalline System. *Z. Naturforsch.* **2003**, *58a*, 45−50.

(18) Allen, F. H. The Cambridge Structural Database: A Quarter of a Million Crystal Structures and Rising. *Acta Crystallogr.* **2002**, *B58*, 380−388.

(19) Dolder, S.; Liu, S.-X.; Guégano, X.; Atanasov, M.; Daul, C. A.; Leiggener, C.; Hauser, A.; Neels, A.; Decurtins, S. Preparation and Characterization of 3-(4,5-Ethylenedithio-1,3-dithiol-2-ylidene)-naphthopyranone: A Luminescent Redox-Active Donor−Acceptor Compound. *Tetrahedron* **2006**, *62*, 11106−11111.

(20) (a) Fock, M. V. The Separation of Compound Spectra into Individual Bands with Assistance of Generalized Alentsev methods. *Trudy FIAN* **1972**, *59*, 3−24. (b) Sunshine, J. M.; Pieters, C. M.; Pratt, S. F. Deconvolution of Mineral Absorption Bands: An Improved Approach. *J. Geophys. Res.* **1990**, *95* (B5), 6955−6966. (c) Kuznetsov, V. N.; Ryabchuk, V. K.; Emeline, A. V.; Mikhaylov, R. V.; Rudakova, A. V.; Serpone, N. Thermo- and Photo-stimulated Effects on the Optical Properties of Rutile Titania Ceramic Layers Formed on Titanium Substrates. *Chem. Mater.* **2013**, *25*, 170−177.

(21) Demeter, A.; Berces, T.; Biczok, L.; Wintgens, V.; Valat, P.; Kossanyi, J. Comprehensive Model of the Photophysics of *N*-Phenylnaphthalimides: The Role of Solvent and Rotational Relaxation. *J. Phys. Chem.* **1996**, *100*, 2001−2011.

(22) (a) Hoa, G. H. B.; Kossanyi, J.; Demeter, A.; Biczók, L.; Bérces, T. Pressure Dependence of the Dual Luminescence of Twisting Molecules. The Case of Substituted 2,3-Naphthalimides. *Photochem. Photobiol. Sci.* **2004**, *3*, 473−482. (b) Cao, H.; Chang, V.; Hernandez, R.; Heagy, M. D. Matrix Screening of Substituted *N*-Aryl-1,8-naphthalimides Reveals New Dual Fluorescent Dyes and Unusually Bright Pyridine Derivatives. *J. Org. Chem.* **2005**, *70*, 4929−4934. (c) Paudel, S.; Nandhikonda, P.; Heagy, M. D. A Comparative Study into Two Dual Fluorescent Mechanisms via Positional Isomers of *N*-hydroxyarene-1,8-naphthalimides. *J. Fluoresc.* **2009**, *19*, 681−691. (d) Nandhikonda, P.; Begaye, M. P.; Cao, Z.; Heagy, M. D. Frontier Molecular Orbital Analysis of Dual Fluorescent Dyes: Predicting Two-Color Emission in *N*-Aryl-1,8-naphthalimides. *Org. Biomol. Chem.* **2010**, *8*, 3195−3201. (e) Duke, R. M.; Gunnlaugsson, T. 3-Urea-1,8-naphthalimides Are Good Chemosensors: A Highly Selective Dual Colorimetric and Fluorescent ICT Based Anion Sensor for Fluoride. *Tetrahedron Lett.* **2011**, *52*, 1503−1505. (f) Guo, T.; Cui, L.; Shen, J.; Wang, R.; Zhu, W.; Xu, Y.; Qian, X. A Dual-Emission and Large Stokes Shift Fluorescence Probe for Real-Time Discrimination of ROS/RNS and Imaging in Live Cells. *Chem. Commun.* **2013**, *49*, 1862−1864.

(23) Inoue, Y.; Jiang, P.; Tsukada, E.; Wada, T.; Shimizu, H.; Tai, A.; Ishikawa, M. Unique Dual Fluorescence of Sterically Congested Hexaalkyl Benzenehexacarboxylates: Mechanism and Application to Viscosity Probing. *J. Am. Chem. Soc.* **2002**, *124*, 6942−6949.

(24) Matsubayashi, K.; Shiratori, H.; Kubo, Ya. Effect of Addition of Trifluoroacetic Acid on the Photophysical Properties and Photo-reactions of Aromatic Imides. *Tetrahedron* **2010**, *66*, 9291−9296.

(25) Prunkl, Ch.; Pichlmaier, M.; Winter, R.; Kharlanov, V.; Rettig, W.; Wagenknecht, H.-A. Optical, Redox, and DNA-Binding Properties of Phenanthridinium Chromophores: Elucidating the Role of the Phenyl Substituent for Fluorescence Enhancement of Ethidium in the Presence of DNA. *Chem.—Eur. J.* **2010**, *16*, 3392−3402.

(26) Nandhikonda, P.; Heagy, M. D. Dual Fluorescent *N*-Aryl-2,3-naphthalimides: Applications in Ratiometric DNA Detection and White Organic Light-Emitting Devices. *Org. Lett.* **2010**, *12*, 4796−4799.

(27) Granzhan, A.; Ihmels, H.; Viola, G. 9-Donor-Substituted Acridizinium Salts: Versatile Environment-Sensitive Fluorophores for the Detection of Biomacromolecules. *J. Am. Chem. Soc.* **2007**, *129*, 1254−1267.

(28) (a) Ingrassia, L.; Lefranc, F.; Kiss, R.; Mijatovic, T. Naphthalimides and Azonafides as Promising Anti-Cancer Agents. *Curr. Med. Chem.* **2009**, *16*, 1192−1213. (b) Tumiatti, V.; Milelli, A.; Minarini, A.; Micco, M.; Gasperi Campani, A.; Roncuzzi, L.; Baiocchi, D.; Marinello, J.; Capranico, G.; Zini, M.; et al. Design, Synthesis, and

Biological Evaluation of Substituted Naphthalene Imides and Diimides as Anticancer Agent. *J. Med. Chem.* **2009**, *52*, 7873−7877.
(29) Frisch, M. J.; Trucks, G. W.; Schlegel, H. B.; Scuseria, G. E.; Robb, M. A.; Cheeseman, J. R.; Scalmani, G.; Barone, V.; Mennucci, B.; Petersson, G. A.; et al. *Gaussian 09*, revision C.1; Gaussian, Inc.: Wallingford CT, 2009.
(30) Yanai, T.; Tew, D.; Handy, N. A New Hybrid Exchange−Correlation Functional Using the Coulomb-Attenuating Method (CAM-B3LYP). *Chem. Phys. Lett.* **2004**, *393*, 51−57.
(31) (a) Jacquemin, D.; Perpète, E. A.; Scalmani, G.; Ciofini, I.; Peltier, C.; Adamo, C. Absorption and Emission Spectra of 1,8-Naphthalimide Fluorophores: A PCM-TD-DFT Investigation. *Chem. Phys.* **2010**, *372*, 61−66. (b) Kucheryavy, P.; Li, G.; Vyas, S.; Hadad, C.; Glusac, K. D. Electronic Properties of 4-Substituted Naphthalimides. *J. Phys. Chem. A* **2009**, *113*, 6453−6461.
(32) Marenich, A. V.; Cramer, C. J.; Truhlar, D. G. Universal Solvation Model Based on Solute Electron Density and on a Continuum Model of the Solvent Defined by the Bulk Dielectric Constant and Atomic Surface Tensions. *J. Phys. Chem. B* **2009**, *113*, 6378−6396.
(33) El-Sayed, M. A. Spin—Orbit Coupling and the Radiationless Processes in Nitrogen Heterocyclics. *J. Chem. Phys.* **1963**, *38* (12), 2834 (5 pages)..
(34) Toro, C.; De Boni, L.; Yao, S.; Ritchie, J. P.; Masunov, A. E.; Belfield, K. D.; Hernandez, F. E. Linear and Nonlinear Optical Characterization of a Monomeric Symmetric Squaraine-Based Dye in Solution. *J. Chem. Phys.* **2009**, *130*, 214504 (6 pages).
(35) Masunov, A.; Tretiak, S.; Hong, J. W.; Liu, B.; Bazan, G. C. Theoretical Study of the Effects of Solvent Environment on Photophysical Properties and Electronic Structure of Paracyclophane Chromophores. *J. Chem. Phys.* **2005**, *122*, 10 Article Number: 224505 (10 pages).
(36) Cheshmedzhieva, D.; Ivanova, P.; Stoyanov, S.; Tasheva, D.; Dimitrova, M.; Ivanov, I.; Ilieva, S. Experimental and Theoretical Study on the Absorption and Fluorescence Properties of Substituted Aryl Hydrazones of 1,8-Naphthalimide. *Phys. Chem. Chem. Phys.* **2011**, *13*, 18530−18538.
(37) Dashevskij, M. M. *Acenaphtene. M: Chemistry*; 1966; 460 pp.
(38) Ganin, E. V.; Makarov, V. F.; Luk'yanenko, N. G.; Kotlyar, S. A. Acylation of Aza Crown Ethers with *N*-Substituted Isophthalimides. *Chem. Heterocycl. Compd.* **1987**, *23*, 447−450.
(39) Malinovskii, S. T.; Simonov, Yu. A.; Ganin, E. V. Crystal Structures of *N*-Phenyl-2-(1,4,7,10-tetraoxa-13-azacyclopentadecane-13-carbonyl)benzamide and *N*-(4-Ethoxyphenyl)-2-(1,4,7,10-tetraoxa-13-azacyclopentadecane-13-carbonyl)benzamide. *Crystallogr. Rep.* **2001**, *46*, 419−424. (translated from *Kristallografiya* **2001**, *46*, 469-474).